Geosci. Instrum. Method. Data Syst., 13, 277–287, 2024
https://doi.org/10.5194/gi-13-277-2024

Geoscientific Instrumentation Methods and Data Systems
Open Access
EGU

Study on the influence of topography on wind shear numerical simulations based on WRF–CALMET

Xingyu Wang, Yuhong Lei, Baolong Shi, Zhiyi Wang, Xu Li, and Jinyan Wang

Key Laboratory of Climate Resource Development and Disaster Prevention in Gansu Province, College of Atmospheric Sciences, Lanzhou University, Lanzhou 730000, China

Correspondence: Jinyan Wang (wangjny@lzu.edu.cn)

Received: 29 February 2024 – Discussion started: 22 March 2024
Revised: 28 June 2024 – Accepted: 10 July 2024 – Published: 16 September 2024

Abstract. This study focuses on the critical issue of low-altitude wind shear, which is vital for aircraft safety during takeoff and landing. Using the WRF–CALMET model, we assess the impact of topography on low-level wind shear at Zhongchuan Airport. CALMET outperforms WRF, showing improved simulation accuracy. CALMET's simulation highlights diurnal variations in vertical wind shear, which are especially pronounced from 13:00 to 24:00 CST (China standard time, UTC+8). Notably, CALMET indicates wind shear that is one to two hazard levels higher for aircraft operations compared to WRF over a significant area. Terrain sensitivity experiments reveal CALMET's responsiveness to terrain changes during high-wind-shear periods, with reduced impact at higher altitudes. CALMET's incorporation of kinematic terrain influences, blocking effects, slope flow, and strengthened diversion of near-surface airflow on complex terrain contribute to these findings. This study confirms the efficacy of CALMET in simulating low-altitude wind shear, emphasizing its superiority in capturing terrain influences and reducing the aviation safety threat posed by low-altitude wind shear.

1 Introduction

According to the definition of the International Civil Aviation Organization (ICAO), low-level wind shear refers to the sharp change in spatial wind speed or direction within a 600 m altitude range. Wind shear includes both vertical and horizontal components and typically occurs near fronts, coastlines, and the surface. In the process of taking off and landing, low-level wind shear will affect the airspeed of the aircraft, causing great risks and even terrible accidents in serious cases (Evans and Turnbull, 1989). In June 1975, a Boeing 727 aircraft crashed during its landing at Kennedy Airport due to encountering low-level wind shear, resulting in 113 fatalities and 11 injuries (Fujita and Caracena, 1977). In June 2000, a Wuhan Airlines aircraft crashed during landing, also due to encountering low-level wind shear. In 2017, a New Zealand Airlines A320-200 aircraft experienced low-level wind shear during landing, resulting in severe damage to the aircraft and significant economic losses. Therefore, accurate simulation and prediction of low-level wind shear, especially on complex terrain, is of great significance for ensuring the safety of aircraft takeoffs and landings at airports.

However, achieving accurate predictions remains a primary challenge faced by numerical weather forecasting models (Colman et al., 2012). Low-level wind shear is influenced by multiscale weather systems and characterized by small temporal and spatial scales, high intensity, and sudden occurrences, thus making it difficult to detect, study, and predict. In simulating actual wind fields, simple characteristics are insufficient; the wind field structure around the airport must be included. There are three main methods for calculating wind shear in model wind fields (Zhang and Jia, 2022). (1) The first method is uses meteorological radar networks and various monitoring networks around airports, where differential methods are employed to collect measured data and record wind speed and direction in a grid format. However, these measurements are scattered and small and are thus insufficient to capture the essential characteristics and dynamic development of low-level wind shear, and they also do not vary with meteorological conditions. (2) The second type of wind shear model is common in engineering and consists of

simple models. These typically comprise some physical concepts, represented through simple mathematical fitting and basic fluid dynamics solutions. They only reflect essential features of the wind shear field without fully capturing the true wind field characteristics (Li et al., 2018). (3) The third type of wind shear model is based on atmospheric dynamics and physical equations and is solved directly by large computers. Among these methods, the third not only simulates the real wind shear in the wind field but also provides other useful physical quantities (e.g., temperature, water content, and radar reflectivity), revealing the formation process, causes, and development of wind shear. Many studies have utilized numerical models to simulate low-level wind shear.

Boilley and Mahfouf (2023) used the non-hydrostatic Meso-NH model to simulate two different wind shear events in the complex terrain around Nice Côte d'Azur Airport. They successfully predicted vertical wind shear and local turbulence; however, due to the model resolution limitation (500 m), the study did not accurately predict the time and location of low-level wind shear. Consequently, subsequent wind shear studies have continuously improved spatial resolution. The Weather Research and Forecasting (WRF) model, designed for high-resolution mesoscale weather forecasting, simulates airflow under realistic atmospheric conditions. However, due to the grid resolution of WRF being greater than 1 km, it struggles to simulate the small-scale airflow movements in complex terrain. Hong Kong International Airport previously attempted to predict wind shear using the WRF model, affirming its capability to forecast wind shear induced by terrain changes several hours in advance, and studied the model's performance under non-temperature inversion conditions, where it reproduced wind shear characteristics well. However, providing precise warnings for the airport proved challenging (Chan and Hon, 2016). Building on this, Hong Kong International Airport conducted further research: using a 200 m resolution numerical weather prediction model (AVM) designed for fine short-term weather forecasting based on WRF3.4.1, during the whole research period the results were consistent with the model forecast as observed on both runways (Hon, 2020). Since then, Hong Kong International Airport improved the WRF-based coupled model, utilizing the WRF–LES coupled model to capture many wind characteristics and microscale airflow within the airport, accurately reproducing real wind direction changes (Chen et al., 2022). These studies demonstrate the effectiveness of numerical models in simulating low-level wind shear in airport regions, with higher-resolution models providing better simulation results. The series of studies conducted at Hong Kong International Airport suggests that improving models based on the WRF model or coupling it with other models is a promising approach for studying low-level wind shear. In previous studies, the WRF–CALMET coupled model has never been used to study low-level wind shear in airport regions. This study uses this model, significantly improving simulation resolution and leveraging CALMET's advantages in wind field calculations, providing a new method for numerical simulation of low-level wind shear in airport areas.

Lanzhou Zhongchuan International Airport stands as one of the largest aviation hubs in northwestern China, situated in the southeastern part of the Qinwangchuan alluvial-fan basin, surrounded by mountains on all sides. The region is known for frequent wind shear occurrences, a phenomenon that has become increasingly common at Lanzhou Zhongchuan Airport due to the rapid growth in the number of flights. Most wind shear events occur during spring and summer, particularly in May, June, and July (Li et al., 2020). Statistical reports on wind shear at Lanzhou Zhongchuan Airport indicate that the majority of incidents occur in the afternoon and evening. This trend is attributed to the downward momentum in the afternoon, enhanced convective activity from increased ground heating, and higher wind speeds. Severe convective weather is more likely to occur in the late afternoon to evening, contributing to a higher frequency of reported low-level wind shear events. Conversely, fewer flights operate during the night, accompanied by reduced convective weather, resulting in relatively few reports of aircraft encountering low-level wind shear (Dang et al., 2013). In May 2016, Zhongchuan Airport installed coherent Doppler lidar near the runway to study the characteristics of low-level wind shear and provide warnings (Li et al., 2020). Numerical simulation studies on wind shear at Zhongchuan Airport have been ongoing. Jiang et al. (2018) selected a 6 km × 6 km area near the runway at Zhongchuan Airport to establish a digital elevation model of the terrain. They used FLUENT software for numerical simulation, solving iterative calculations to obtain the distribution characteristics of wind speed and pressure in the simulated area. However, FLUENT, being a computational fluid dynamics (CFD) simulation software widely used in engineering, science, and research fields, only considers the local turbulence of terrain and buildings on the flow field. It does not account for factors such as gravity and heat exchange in real atmospheric conditions. Therefore, relying solely on FLUENT for simulating and warning wind shear at Zhongchuan Airport has its limitations. Improvements in simulating low-level wind shear still require enhancements built upon numerical weather forecasting models.

In both domestic and international research, the CALMET model is frequently employed to downscale WRF, providing a finer representation of microscale terrain structures. Particularly in weak wind conditions, the CALMET downscaling coupling model outperforms WRF in simulating near-surface wind directions (Zhang et al., 2020). The WRF–CALMET coupled system demonstrates satisfactory performance in various challenging scenarios, including the complex terrain of the Qinghai-Tibet Plateau (Liao et al., 2021) and the intense weather system of Super Typhoon Meranti (2016) (Tang et al., 2021). Up to now, no one has used WRF–CALMET coupling system to simulate and test the occurrence of low-altitude wind shear. Therefore, this study

Table 1. Model configuration.

Physical scheme	WRF option
Microphysics	Thompson graupel scheme (two-moment scheme in V3.1)
Cumulus parameterization	Tiedtke scheme
Longwave radiation	RRTMG
Shortwave radiation	RRTMG
Surface layer	Monin–Obukhov (Janjić Eta) scheme
Land surface	Noah
Boundary layer	MYJ

leveraged the dynamic downscaling effect of the CALMET model on local micro-terrain to achieve high-resolution wind shear simulations with relatively low computational requirements within a small area. Additionally, we conducted controlled variable experiments by modifying the original terrain. This approach has not been attempted in studies investigating terrain-induced wind shear at other airports. It provides an improved method for simulating low-level wind shear within the WRF model.

2 Mode, data, method, and experimental setup

2.1 Models and experimental setup

In this study, the WRF model (version 4.2) was employed to simulate a severe convective weather event occurring in the vicinity of Zhongchuan Airport over a duration of 96 h, starting from 2 July 2022, at 00:00 UTC. The simulated wind field results were then downscaled to 100 m through coupling with the CALMET model. The model utilized a three-layer, two-way nested domain configuration (Fig. 1a), with horizontal grid spacings of 9, 3, and 1 km. In the vertical direction, there were 39 complete Eta layers from the surface to 0 hPa. The physical schemes employed by WRF are detailed in Table 1.

The diagnostic model utilized in this research is the CALMET model (version 6.5), which constitutes the meteorological component of the California Puff Dispersion Model (Scire et al., 2000). In the configuration of this study, the initial guessed wind field is obtained from the grid wind field generated by the innermost domain of WRF, with a horizontal grid spacing of 1 km (D3 in Fig. 1a). Since no objective analysis procedure is employed, we only pay attention to the first step wind field. The coverage area of the CALMET model encompasses Zhongchuan Airport and its surrounding 38 km × 38 km region (Fig. 1b), with a horizontal resolution of 100 m. The vertical layers are set to 10 height levels within 600 m from the ground (the height range influenced by low-level wind shear).

Terrain Sensitivity experiments for demonstrating the impact of terrain on wind shear simulation in CALMET.

1. *CALMET.* The CALMET model configured with default settings as described above.
2. *CALMET_FLAT.* Modification in the TERREL terrain processing module where the elevation of all grid points is adjusted to 2000 m. This adjustment facilitates CALMET simulation on a flat underlying surface.
3. *CALMET_RAISE.* Modification in the TERREL terrain processing module where the elevation of grid points with an altitude exceeding 2050 m is increased by 1.5 times. This modification enables CALMET to simulate wind shear over a more rugged terrain.

These terrain sensitivity experiments are designed to showcase how variations in terrain impact wind shear simulation within CALMET. The CALMET_FLAT experiment simulates wind shear on a flat surface, while the CALMET_RAISE experiment explores wind shear simulation over steeper terrain. The comparison of results from these experiments with the default CALMET setting will provide insights into the sensitivity of wind shear simulations to terrain variations.

2.2 Data

The terrain data come from the global 90 m digital elevation dataset of Shuttle Radar Topography (SRTM3 V4.1) of NASA, and the land use data come from the global land cover type data with 10 m resolution of Pengcheng Laboratory (https://www.pcl.ac.cn/html/1030/) of Tsinghua University in 2017.

The horizontal resolution of the ECMWF Reanalysis v5 (ERA5) dataset is 0.25° × 0.25°, with a temporal resolution of 1 hour. This dataset is employed as both the initial input and boundary fields for WRF model. Additionally, this study utilizes ERA5 variables, specifically geopotential height and temperature, for analyzing weather systems during periods of intense convection.

Observational data for ground-level 10 m wind speed at Lanzhou Zhongchuan Airport are sourced from historical wind speed records provided by the National Oceanic and Atmospheric Administration (NOAA) (https://www.ncei.noaa.gov/maps/daily/, last access: 9 July 2024) with a temporal resolution of 1 h. The ground 10 m wind speed data of the WRF model, CALMET model, and ERA5 reanalysis are interpolated to the location of Zhongchuan Airport and compared with the observed data to verify the performance of the models.

2.3 Method

To quantify the differences in 10 m wind speed among the experiments, the following statistical metrics are employed.

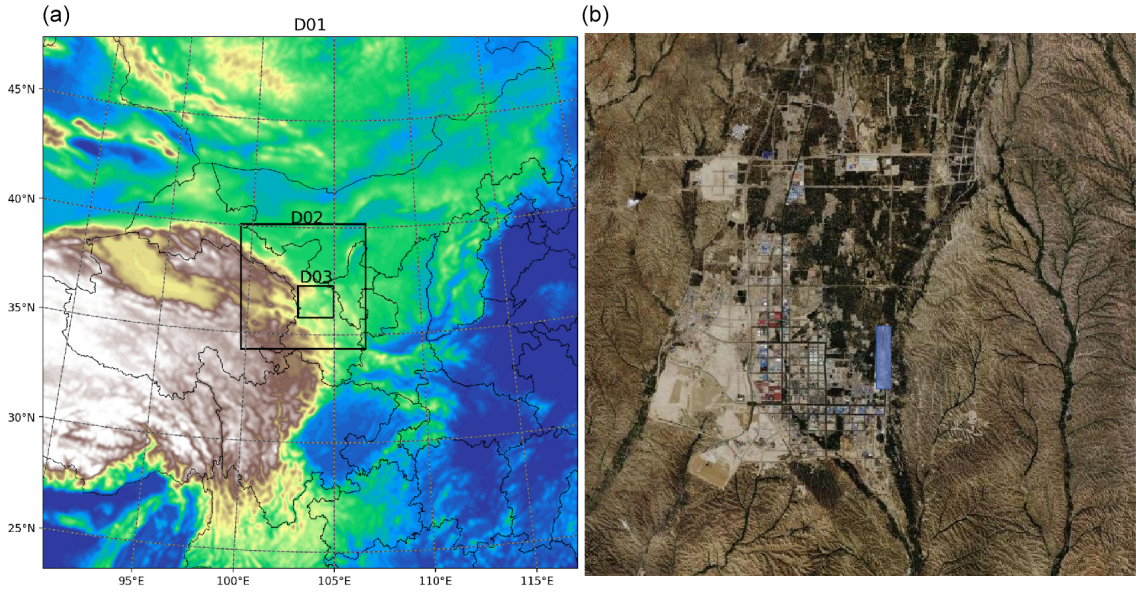

Figure 1. Three-layer nested domains of the WRF Model **(a)** and the simulation area of the CALMET Model (© Google Maps) **(b)**, with Zhongchuan Airport Highlighted in blue.

Index of agreement (IA):

$$\mathrm{IA} = 1 - \frac{\sum_{i=1}^{N}(P_i - O_i)^2}{\sum_{i=1}^{N}\left(\left|P_i - \overline{O}\right| + \left|O_i - O\right|\right)^2}. \quad (1)$$

Root-mean-squared error (RMSE):

$$\mathrm{RMSE} = \sqrt{\frac{1}{n}\sum_{i=1}^{n}(O_i - P_i)^2}. \quad (2)$$

Mean relative error (MRE):

$$\mathrm{MRE} = \frac{1}{n}\sum_{i=1}^{n}\frac{(P_i - O_i)}{O_i}. \quad (3)$$

Here, $\overline{O}$ and $\overline{P}$ represent the average values of observational and simulated data, respectively. Each observed value is denoted as O_i, and each simulated value is denoted as P_i. Smaller values for MRE and RMSE and an IA closer to 1.0 indicate better simulation performance.

Wind shear can be categorized into three types: vertical shear β, meridional horizontal shear α_1, and zonal horizontal shear α_2. Among these, vertical shear of horizontal wind has a more significant impact on aircraft takeoff and landing compared to the other types (Bretschneider et al., 2022). It results in changes in wind speed and direction as an aircraft moves through different altitudes, which can lead to drastic changes in airflow during ascent or descent, thereby increasing flight difficulty, particularly during takeoff and landing (Keohan, 2007; Eggers et al., 2003).

3 Results

3.1 Improvement of the WRF–CALMET coupling model for simulation of low-level wind shear

We evaluated the performance of two models in simulating near-surface wind speeds, as shown in Fig. 2 and Table 2. Both models showed better agreement with observed data during periods of low wind speeds before convective development (06:00 CST, China standard time, on 3 July) and after convective cessation (02:00 on 5 July). During periods of intense convection, both models captured wind speed variability. Although both experiments underestimated or overestimated peak wind speeds on 3 and 4 July, CALMET slightly outperformed WRF in simulating high wind speeds. Furthermore, Table 2 indicates that CALMET's mean relative error and root-mean-squared error were lower than those of WRF throughout the entire simulated period, with improvements of 11.13 % and 7.24 %, respectively. CALMET's index of agreement was also closer to 1 compared to the WRF experiment, with an improvement of 12.06 %. These results demonstrate CALMET's superior overall simulation performance compared to WRF.

At 16:00 on 3 July, significant fluctuations in surface wind speeds mark the onset of convective development (Fig. 2). Figure 3 illustrates the distribution of vertical wind shear (VWS) simulated by both models. In the layer between 10 and 30 m above ground level, CALMET's maximum VWS values, while consistent in location with WRF's, are notably higher. Terrain analysis reveals CALMET simulates high VWS values near mountain foothills and western slopes (Fig. 6). WRF's high VWS values primarily occur in moun-

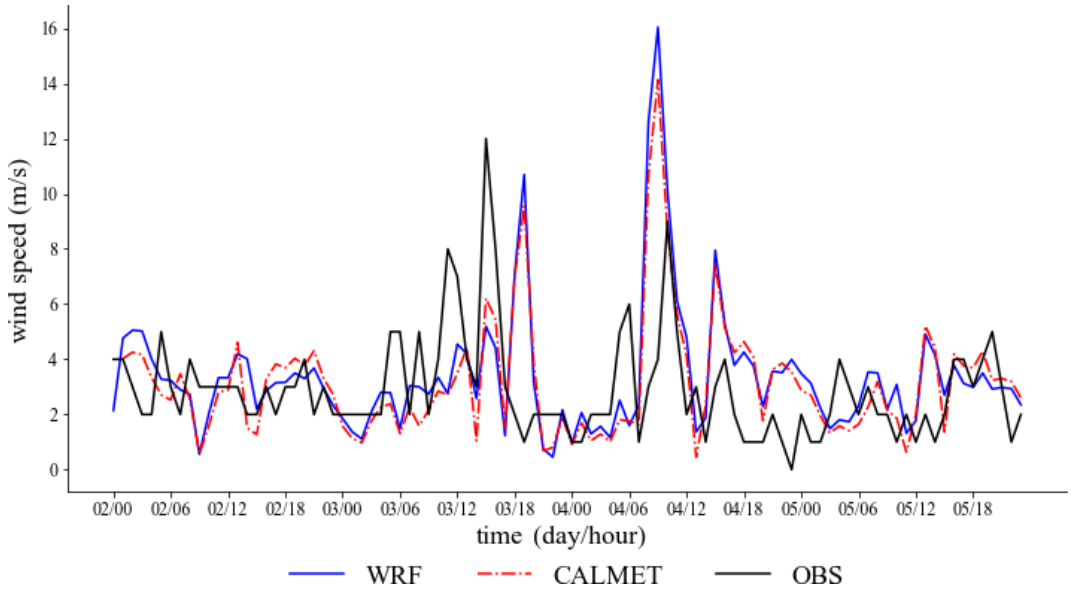

Figure 2. The time series of 10 m surface wind speed for both numerical simulations and observational data.

Table 2. Averaged statistical results of near-surface wind speed simulations in different experiments.

	WRF	CALMET	Improvement (%)
MRE (%)	43.255	38.425	11.13
RMSE ($m\,s^{-1}$)	2.713	2.517	7.24
IA	0.454	0.509	12.09

tainous regions. Details for the height layers of 200–300 and 500–600 m can be found in the Supplement. Overall, both models exhibit decreasing VWS with increasing height. From the overall distribution of VWS, CALMET can simulate a wider range of third- and fourth-level wind shears, which are associated with severe and extreme turbulence affecting aircraft takeoff and landing. Furthermore, this capability provides valuable warnings for aircraft operations at Nakawa Airport.

The atmosphere above and surrounding the mountainous terrain is characterized by three distinct regions or inclined layers, comprising the thermal structure undergoing diurnal variations and forming diurnal winds: slope atmosphere, valley atmosphere, and mountain atmosphere (Zardi and Whiteman, 2012; White, 1992). It is challenging to observe any pure form of diurnal mountain wind system, as each component interacts with the others. Well-organized thermally driven flows can be identified over a broad spatial scale, ranging from the dimensions of the largest mountain ranges to the smallest local topography. Therefore, concerning wind shear in mountainous and foothill areas, wind shear in mountainous areas tends to be smaller. When airflow passes through mountain ridges, the lower-level airflow experiences significant compression. According to the conservation of flux, the acceleration effect on lower-level airflow exceeds that on upper-level airflow, resulting in an overall reduction in wind shear. When the acceleration effect on lower-level airflow is significant while the upper-level acceleration effect is weak or absent, negative wind shear occurs. Overall, the intensity of low-level wind shear may be greater near mountain foothills or ridges and lesser in valleys or slopes. Hence, the regions of maximum wind shear simulated by CALMET near mountain foothills or ridges are more consistent with reality than those by WRF.

Figure 4 presents the time series of maximum VWS simulated by WRF and CALMET. It can be observed that both WRF and CALMET simulations exhibit a clear diurnal pattern in maximum VWS: maximum values are relatively small around dawn and in the morning (01:00 to 12:00), with minimal fluctuations, while they increase significantly in the afternoon and evening (13:00 to 24:00), showing larger variations. However, the maximum values simulated by WRF are generally lower than those by CALMET, with this difference being more pronounced in the afternoon and evening. On 3 and 4 July, during periods of intense convective activity, CALMET is able to simulate larger fluctuations in maximum VWS compared to normal conditions.

In summary, utilizing CALMET for downscaling WRF output of wind fields provides higher resolution and more precise surface conditions, which are advantageous for simulating mesoscale wind shear. This is primarily manifested in the following aspects: the distribution of VWS in the mid-to-low levels is more significantly influenced by terrain, and VWS decreases more rapidly with increasing altitude; the diurnal variation of maximum VWS within VWS regions fol-

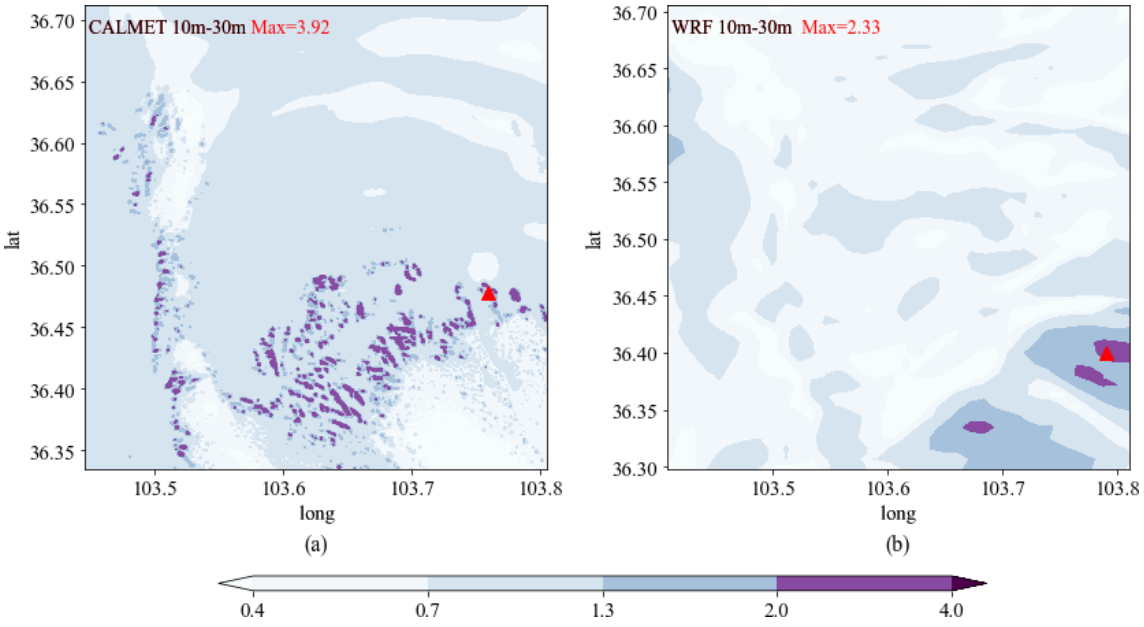

Figure 3. Vertical wind shear (VWS) at 16:00 on 3 July 2022, simulated by CALMET **(a)** and WRF **(b)** ($m\,s^{-1}$ $10\,m^{-1}$). Triangles indicate the locations of maximum values.

lows a clear pattern and can reflect the characteristics of intense convection.

3.2 Impact of topography on wind shear simulation

Through different terrain configurations, we explored CALMET's detailed terrain impact on low-level wind shear. We found that valley winds affect VWS diurnal variation. Terrain, blocking effects, and slope flow kinematics enhance near-surface airflow diversion, deflection, and ascent over complex terrain, significantly influencing VWS, with the impact decreasing with height.

In the CALMET_FLAT experiment, the increase in maximum VWS during the afternoon and evening is minimal (Fig. 4), with slight fluctuations and values around $2\,m\,s^{-1}$ $10\,m^{-1}$, sometimes even lower than WRF. However, good agreement is observed among the three experiments during the early morning and morning periods. In CALMET_RAISE, particularly on 3 and 4 July during intense convective development, fluctuations in the afternoon and evening are more pronounced compared to CALMET. However, CALMET_RAISE shows stability similar to CALMET just before convective development on 2 July, except for an unusually high value at 09:00 on 4 July, where fluctuations are more pronounced but numerically close to CALMET.

In the afternoon and evening, CALMET_FLAT shows a significant decrease in maximum VWS, while CALMET_RAISE exhibits more pronounced fluctuations. For example, at 19:00 on 3 July (Fig. 5a–c), in the CALMET experiment, the maximum VWS ($3.56\,m\,s^{-1}$ $10\,m^{-1}$) occurs in the southeastern foothills and valley areas. In CALMET_FLAT, except for the absence of a high-value area in the southeast, the distribution is similar to CALMET, with a maximum value of $1.77\,m\,s^{-1}$ $10\,m^{-1}$ in the central region, which is also a flat valley area in CALMET. In CALMET_RAISE, due to a sudden 1.5-fold increase in terrain elevation above 2050 m, the steep terrain causes chaotic wind shear distribution, with scattered high values in the central region, and the maximum value increases to $4.31\,m\,s^{-1}$ $10\,m^{-1}$. In summary, transitioning from complex to flat terrain shifts the location of maximum VWS from mountainous areas to flat valleys.

This phenomenon is a typical result of valley winds, driven by the interaction between terrain and solar radiation. During the day, sunlight heats the surface, leading to differential heating rates between slopes and valleys due to their distinct topographies. Slopes, receiving direct sunlight, warm up faster than valleys. At night, the surface loses heat, particularly in valleys with good heat dissipation, resulting in strong nighttime cooling effects. The temperature difference between slopes and valleys during the day induces upslope airflow along the slopes. As the heated air ascends, airflow forms over the valleys, as depicted in Fig. 5a, where maximum VWS occurs near mountainous areas. At night, cold air flows downhill along the slopes, forming downslope winds, which reverse the airflow pattern observed during the day.

The results indicate that CALMET model simulations of VWS are highly sensitive to terrain: VWS values are generally lower in flat terrain compared to complex terrain, and the influence of terrain on wind shear diminishes rapidly with height. In extremely steep terrain, near-surface distribution appears chaotic, but VWS values notably increase above the surface compared to complex terrain. Across the three ex-

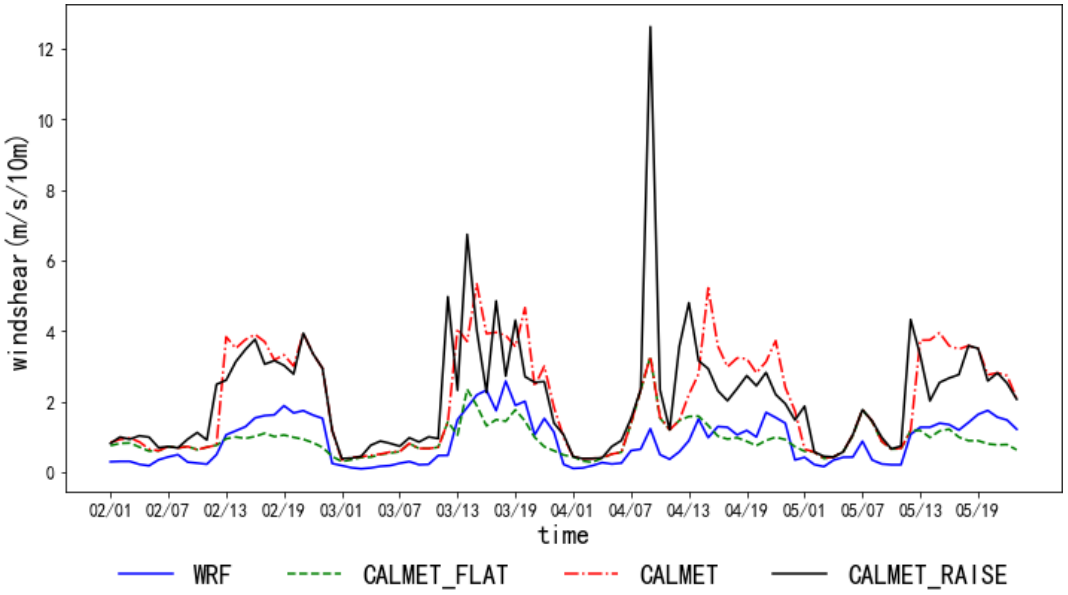

Figure 4. Time series of 10–30 m maximum VWS values of different simulation experiments in the study area.

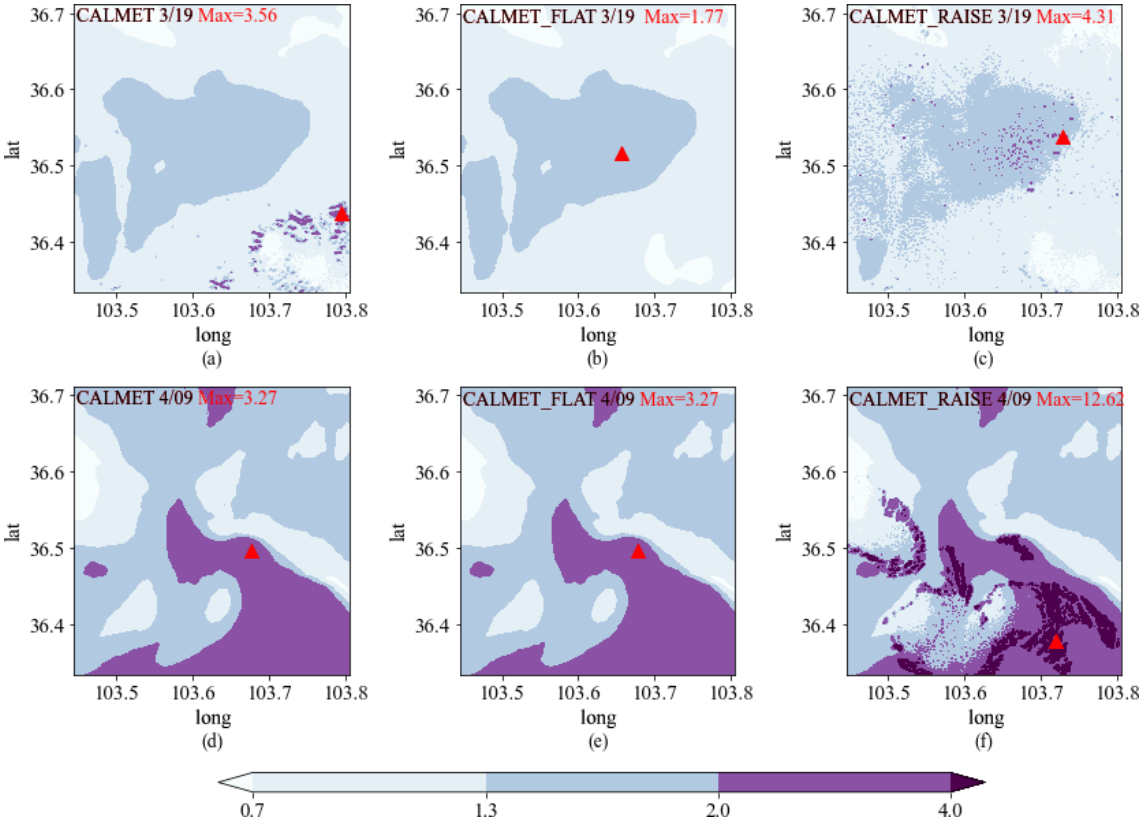

Figure 5. VWS distribution of 10–30 m at **(a–c)** 19:00 on 3 July 2022 and **(d–f)** 09:00 on 4 July 2022 for **(a, d)** CALMET, **(b, e)** CALMET_FLAT, and **(c, f)** CALMET_RAISE.

periments, the absolute differences in VWS decrease with height, suggesting a diminishing impact of terrain on CALMET model simulations of VWS with increasing altitude.

To investigate extreme high values of VWS in the CALMET_RAISE experiment at 09:00 on 4 July, Fig. 5d–f display the VWS distribution for all experiments at this time, while Fig. 6 presents wind vector maps for 3 h for both CALMET and CALMET_RAISE. The VWS distribution for CALMET and CALMET_FLAT is similar, with a peak of $3.27\,m\,s^{-1}\,10\,m^{-1}$ in the central region. Compared to 3 July at 19:00, both experiments show extensive high-value areas in the southeast, with CALMET_RAISE reaching an exceptional maximum of $12.62\,m\,s^{-1}\,10\,m^{-1}$ in the southeastern valley area. Additionally, CALMET_RAISE exhibits large areas of exceptionally high values compared to the other experiments.

In Fig. 6, at 08:00 and 10:00 on 4 July, the prevailing wind direction in the area is northeast. Both CALMET and CALMET_RAISE show similar wind field structures, transitioning from northeast to north as terrain slopes southward. When airflow passes through the southern valley, mountain ranges create denser wind vectors and increased speeds. However, at 09:00, a strong northwest airflow converges with the northern airflow, forming a distinct "micro-front". The terrain blocking induces diversion, deflection, and upward motion of the northwesterly wind, creating extensive high-value VWS areas in the southeast. Compared to CALMET, CALMET_RAISE exhibits a more chaotic wind field due to increased terrain.

In conclusion, the widespread high-value VWS area observed at 09:00 on 4 July resulted from a shift in wind direction to the northwest, encountering minimal velocity reduction before reaching the tall terrain in the south, where the mountainous obstruction led to diversion, deflection, and upward motion. The anomalously high values in the CALMET_RAISE experiment were attributed to the elevation of the terrain, significantly intensifying the effects of diversion, deflection, and upward motion. This suggests that terrain has a more pronounced impact on CALMET-simulated wind shear during high wind speeds, while its influence is less evident during low wind speeds. Therefore, heightened awareness of low-level wind shear occurrence is warranted in complex terrain.

4 Conclusion

In order to investigate whether higher-resolution numerical models yield better simulation results for low-level wind shear, this study focuses on a severe convective weather event that occurred in the vicinity of Zhongchuan Airport on 2 July 2022. The WRF–CALMET coupled model is utilized to simulate the wind field, and the influence of terrain variations on CALMET-simulated wind shear is explored. The main conclusions are as follows.

1. CALMET improves the simulation of near-surface winds, bringing them closer to observed data than WRF, thereby facilitating more accurate modeling of low-level wind shear.

2. The diurnal variation of VWS shows a distinct pattern. CALMET exhibits higher VWS compared to WRF, especially during the afternoon and evening. During periods of intense convective activity, CALMET captures larger VWS fluctuations, including higher peak values. CALMET's finer terrain features result in a VWS distribution that better aligns with terrain effects, with VWS generally higher near foothill areas compared to mountains, and a more pronounced decrease with altitude.

3. Terrain sensitivity experiments show that during early morning and morning hours, the maximum VWS values of the three experiments were similar, occurring in flat regions with minimal terrain influence. However, in the afternoon and evening, CALMET_FLAT shows decreased maximum VWS values, while CALMET_RAISE exhibits drastic fluctuations, with peak values near mountainous areas, indicating significant terrain influence. Moreover, the impact of terrain on CALMET-simulated VWS diminishes with altitude. These findings highlight the substantial influence of terrain on CALMET, particularly during periods of high wind speeds.

4. The occurrence of abnormally high VWS values in the simulations is attributed to strong disturbances caused by tall terrain features: wind direction shifts to northwesterly winds, encountering minimal reduction in wind speed before encountering the tall terrain in the southern region. CALMET_RAISE elevates the terrain from its original level, enhancing channeling, swirling, and updraft effects.

CALMET is a mature dynamic regional downscaling tool, and using other numerical weather prediction models can also achieve the scale of CALMET. We chose to use CALMET for the following reasons: from the perspective of operational considerations, conducting research at the same scale requires lower computational requirements and hardware needs for when using the CALMET model.

The research findings of this study are solely based on a short-term simulation period of weather events in the Zhongchuan Airport area. However, this specific case does not necessarily represent the overall wind shear situation at the airport, as it is just one weather event with significant wind shear. Obtaining radar wind profiler data for the airport poses certain difficulties because we do not have Doppler lidar equipment available. Direct observation of wind shear is challenging. We have made efforts to obtain reanalysis data and site wind speed observations as much as possible. Due to limited funding in the preliminary stages of our research,

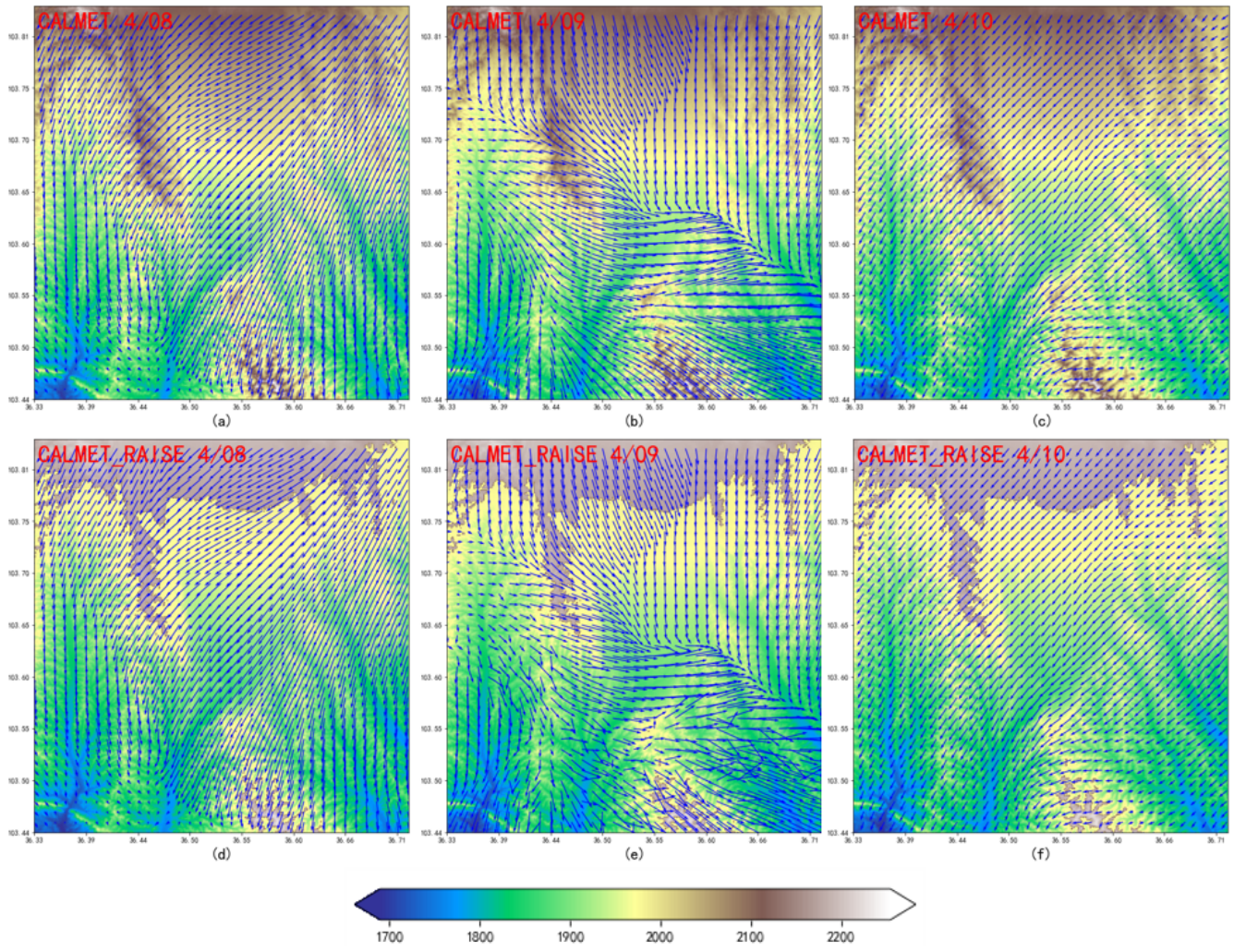

Figure 6. Topographic elevation (m) and wind vector distribution in **(a–c)** CALMET and **(d–f)** CALMET_RAISE at **(a, d)** 08:00 on 4 July, **(b, e)** 09:00 on 4 July, and **(c, f)** 10:00 on 4 July.

we could only start with theoretical studies, and field experiments will be conducted once funding becomes available. Our future work will expand to include longer simulation periods in more airports and regions with complex terrain. This expansion aims to examine and quantify the additional value provided by CALMET in simulating low-level wind shear.

Detailed descriptions of the CALMET model, the method for calculating wind shear, the weather processes during the study period, and additional information on the results will be provided in the Supplement.

Code availability. The WRF code used in this study is available at https://www2.mmm.ucar.edu/wrf/users/download/get_source.html (NCAR, 2023). The CALMET code used in this study is available at https://www.calpuff.org/calpuff/download/mod7_codes.htm (TRC, 2023).

Data availability. The terrain data used in this study come from NASA's Shuttle Radar Topography Mission (SRTM3 V4.1), available at https://app.openskope.org/dataset/srtm (NASA, 2024). The land use data are from the global land cover type data by Pengcheng Laboratory (fromglc10), available at https://www.pcl.ac.cn/html/1030/ (Pengcheng Laboratory, 2024).

Supplement. The supplement related to this article is available online at: https://doi.org/10.5194/gi-13-277-2024-supplement.

Author contributions. All the work of the manuscript was completed by XW, who is also the main author of the manuscript. JW provided critical ideas and numerous improvements for the experiment. YL participated in the development of the Python code for calculating low-level wind shear.

Competing interests. The contact author has declared that none of the authors has any competing interests.

Disclaimer. Publisher's note: Copernicus Publications remains neutral with regard to jurisdictional claims made in the text, published maps, institutional affiliations, or any other geographical representation in this paper. While Copernicus Publications makes every effort to include appropriate place names, the final responsibility lies with the authors.

Acknowledgements. This work was supported by the Joint Funds of the National Natural Science Foundation of China (grant no. U2342205), the Gansu Provincial Association of Science and Technology Innovation Drive Promotion Project (grant no. GXH20230817-7), and the Key Natural Science Foundation of Gansu Province (grant no. 23JRRA1030). We extend our sincere appreciation to the funding agencies for their support.

Additionally, we would like to express our gratitude to the Supercomputing Center of Lanzhou University for their assistance.

Review statement. This paper was edited by Alessandro Fedeli and reviewed by Xiaohang Wen and one anonymous referee.

References

Boilley, A. and Mahfouf, J.-F.: Wind shear over the Nice Côte d'Azur airport: case studies, Nat. Hazards Earth Syst. Sci., 13, 2223–2238, https://doi.org/10.5194/nhess-13-2223-2013, 2013.

Bretschneider, L., Hankers, R., Schönhals, S., Heimann, J.-M., and Lampert, A.: Wind shear of low-level jets and their influence on manned and unmanned fixed-wing aircraft during landing approach, Atmosphere, 13, 35, https://doi.org/10.3390/atmos13010035, 2021.

Chan, P. and Hon, K.: Observation and numerical simulation of terrain-induced windshear at the Hong Kong International Airport in a planetary boundary layer without temperature inversions, Adv. Meteorol., 2016, 1454513, https://doi.org/10.1155/2016/1454513, 2016.

Chen, F., Peng, H., Chan, P.-w., Huang, Y., and Hon, K.-K.: Identification and analysis of terrain-induced low-level windshear at Hong Kong International Airport based on WRF–LES combining method, Meteorol. Atmos. Phys., 134, 60, https://doi.org/10.1007/s00703-022-00899-1, 2022.

Colman, B., Cook, K., and Snyder, B. J.: Numerical weather prediction and weather forecasting in complex terrain, in: Mountain Weather Research and Forecasting: Recent Progress and Current Challenges, Springer, 655–692, https://doi.org/10.1007/978-94-007-4098-3_11, 2012.

Dang, B., Sun, W., Wang, J., Wei, L., Shang, K., Li, J., and Wang, S.: Analysis of low-altitude wind shear cases at Lanzhou Zhongchuan Airport during 2004–2007, J. Lanzhou Univ. (Nat. Sci.), 49, 63–69, 2013.

Eggers Jr, A., Digumarthi, R., and Chaney, K.: Wind shear and turbulence effects on rotor fatigue and loads control, J. Sol. Energ.-T. ASME, 125, 402–409, 2003.

Evans, J. and Turnbull, D.: Development of an automated windshear detection system using Doppler weather radar, P. IEEE, 77, 1661–1673, 1989.

Fujita, T. T. and Caracena, F.: An analysis of three weather-related aircraft accidents, B. Am. Meteorol. Soc., 58, 1164–1181, 1977.

Hon, K. K.: Predicting low-level wind shear using 200-m-resolution NWP at the Hong Kong International Airport, J. Appl. Meteorol. Clim., 59, 193–206, 2020.

Jiang, L., Liu, X., and Li, Z.: Study on the influence of terrain and buildings around Lanzhou Zhongchuan Airport on wind field, Computer and Digital Engineering, 46, 561–565, https://doi.org/10.3969/j.issn.1672-9722.2018.03.030, 2018.

Keohan, C.: Ground-based wind shear detection systems have become vital to safe operations, Icao Journal, 62, 16–19, 2007.

Li, H., Zhou, M., Guo, Q., Wu, R., and Xi, J.: Compressive sensing-based wind speed estimation for low-altitude wind-shear with airborne phased array radar, Multidim. Syst. Sign. P., 29, 719–732, 2018.

Li, L., Shao, A., Zhang, K., Ding, N., and Chan, P.-W.: Low-level wind shear characteristics and lidar-based alerting at Lanzhou Zhongchuan International Airport, China, J. Meteorol. Res., 34, 633–645, 2020.

Liao, R., Fang, X., Liu, H., Zhou, R., Zhang, L., Zhu, Y., Zhang, D., and Meng, F.: Wind characteristic in the complex underlying terrain as studied with CALMET system, J. Phys. Conf. Ser., 2006, 012053, https://doi.org/10.1088/1742-6596/2006/1/012053, 2021.

NASA: Shuttle Radar Topography Mission (SRTM3 V4.1), NASA [data set], https://app.openskope.org/dataset/srtm, last access: 9 July 2024.

NCAR: Weather Research and Forecasting Model (WRF), NCAR [code], https://www2.mmm.ucar.edu/wrf/users/download/get_source.html, last access: 3 June 2023.

Pengcheng Laboratory: Global Land Cover Type Data (fromglc10), Pengcheng Laboratory [data set], https://www.pcl.ac.cn/html/1030/ last access: 9 July 2024.

Scire, J. S., Robe, F. R., Fernau, M. E., and Yamartino, R. J.: A user's guide for the CALMET Meteorological Model, Earth Tech, USA, 37, https://www.researchgate.net/profile/Mark-Fernau/publication/225089751_A_user's_guide_for_the_CALMET_meteorological_model_Version_5/links/00b7d52be041b28a6a000000/A-users-guide-for-the-CALMET-meteorological-model-Version-5.pdf (last access: 12 September 2024), 2000.

Tang, S., Huang, S., Yu, H., Gu, M., and Tang, J.: Impact of horizontal resolution in CALMET on simulated near-surface wind fields over complex terrain during Super Typhoon Meranti (2016), Atmos. Res., 247, 105223, https://doi.org/10.1016/j.atmosres.2020.105223, 2021.

TRC: CALMET Meteorological Model, TCR [code], https://www.calpuff.org/calpuff/download/mod7_codes.htm last access: 3 June 2023.

White, R. J.: Effect of wind shear on airspeed during airplane landing approach, J. Aircraft, 29, 237–242, 1992.

Zardi, D. and Whiteman, C. D.: Diurnal mountain wind systems, in: Mountain Weather Research and Forecasting: Recent Progress and Current Challenges, Springer Atmospheric Sciences, edited by: Chow, F. K., De Wekker, S. F. J., and Snyder, B. J., https://doi.org/10.1007/978-94-007-4098-3_2, 2013.

Zhang, D., Chen, L., Zhang, F., Tan, J., and Wang, C.: Numerical Simulation of Near-Surface Wind during a Severe Wind Event in a Complex Terrain by Multisource Data Assimilation and Dynamic Downscaling, Adv. Meteorol., 2020, 7910532, https://doi.org/10.1155/2020/7910532, 2020.

Zhang, Y. and Jia, M.: Low-level wind shear of wind field modeling and simulation, Research Square, https://doi.org/10.21203/rs.3.rs-2136969/v1, 2022.